Supplementary Materials and Methods for Teh et al., "An *in vivo* reporter to quantitatively and temporally analyze the effects of CDK4/6 inhibitor-based therapies in melanoma."

Western blot antibodies
Phospho-RB1 (S780) (#9307), RB1 (#9309), p15INK4B (#4822), p16INK4A (#4824), p18INK4C (#2896), cleaved PARP (#9541), cleaved-caspase 3 (#9661), survivin (#2808), BCL-2 (#2870), ERBB3 (#4754), SOX2 (#3579) and SOD2 (#13141) antibodies were purchased from Cell Signaling Tech, Inc. (Danvers, MA). CDK4 (sc-260-G), CDK6 (sc-7181), cyclin A (sc-751) and cyclin D1 (sc-718) antibodies were purchased from Santa Cruz Biotechnology, Inc. (Dallas, TX). Actin (A2066) and fibronectin (F3648) antibodies were purchased from Sigma-Aldrich Co (St. Louis, MO). Bim/BOD antibody (ADI-AAP-330) was purchased from Enzo Life Sciences (Farmingdale, NY).

Pharmacokinetic Study
Immunodeficient nude mice were treated with control chow (n=2 for day 8 and n=3 for day 15) or CDK4/6 inhibitor (429mg/kg palbociclib) chow (n=5). Blood samples were collected retro-orbitally at two separate time-points: day 8 and day 15. Plasma was separated immediately by centrifugation at 1000 RCF for 10 minutes and stored at -80°C. Analyses of plasma samples were carried out by Integrated Analytical Solutions, Inc. (Berkeley, CA) using LC-MS/MS.

RPPA Heatmap Analysis
Samples were separated based on treatment types. The log2 values for the drug resistant samples were used to perform two sample t-tests with 10,000 permutations, followed by multiple hypothesis test corrections for each drug group comparison. A list of significant antibodies was determined by using positive false discovery rate and fold change cutoffs of 0.05 and 1.5 respectively. Median-polished log2 values of the significant antibodies were used to perform hierarchical clustering. Calculations and images were performed using the mattes, mafdr and clustergram functions in Matlab® (version 2015b).

***In Vivo* Statistical Analysis**
In vivo data has error bars representing SEM. The log-transformed tumor volumes were modeled using linear mixed effects (LME) models adjusting for correlations between repeated measures from the same animal and allowing for the mouse-specific tumor growth trajectories. The fixed effects included the treatment group (control, CDK4/6, MEK, and Combo), Day, Day^2, Day^3 and interaction between treatment group and each power of the Day variable. That is, the Day-dependent trends were modeled as cubic polynomials in Day and coefficients for linear, quadratic, and cubic terms were allowed to be different in different treatment groups. The models also allowed for different variances of the errors in different treatment groups since even after the log transformation there were still heteroscedasticty in the errors from different treatment groups. The overall comparisons of the treatment groups (combo vs. single agents) were performed in terms of the time trends, testing the null hypotheses that the coefficients for linear, quadratic and cubic Day terms are equal for the corresponding treatment groups.

The derivative function (quadratic polynomial) for each treatment group was computed from the fitted cubic curve in each treatment group.

Pathway Analysis

ToppGene (accessed 21 March 2016) was used to determine statistically significant up and down regulated pathways for comparisons between each drug resistant group. Cumulative distribution function was used to calculate the statistical significance of pathways from the Reactome pathway database. Pathways were classified as significant by using a Benjamini Hochberg positive false discovery rate cutoff of 0.001.

Supplemental Figure Legends for Teh et al., "An *in vivo* reporter to quantitatively and temporally analyze the effects of CDK4/6 inhibitor-based therapies in melanoma."

Supplemental Table 1. Summary of melanoma cell lines grouped for mutations in CDKN2A, CDK4, BRAF and NRAS. ND: not determined.

Supplemental Figure 1. Low concentrations of palbociclib (0.05 µM) inhibited phosphorylation of RB1 and cyclin A2 expression in sensitive cell lines (GI50<1.5 µM) but not in less sensitive lines.

Supplemental Figure 2. Mean plasma concentration for palbociclib. Mice were treated with control chow or palbociclib for 8 or 15 days.

Supplemental Figure 3. Sensitivity of melanoma cells to trametinib. GI50 values were generated from dose-dependent curves from MTT cell viability assays. Each bar represents the average of three independent experiments.

Supplemental Figure 4. Enhanced PARP cleavage in BRAF and NRAS mutant cells treated with trametinib (5 nM) or trametinib plus palbociclib (0.5 µM).

Supplemental Figure 5. Clustergram and scatter plot generated from apoptosis PCR Array. A375 and SBcl2 cells were treated as indicated for 24 hours.

Supplemental Figure 6. Endogenous levels of survivin in a panel of melanoma cell lines.

Supplemental Figure 7. Representative tumor size of 1205Lu xenografts measured by tdTomato fluorescence activity (error bars represent SEM, *p<0.0001 comparing combo to control, CDK4/6i and MEKi).

Supplemental Figure 8. Average weight (g) of mice bearing 1205Lu xenografts treated in each cohort (n=6 in control, n=10 in MEKi, n=9 in CDK4/6i, n=9 in COMBOi, error bars represent SD). The weight was comparable between each treatment groups.

Supplemental Figure 9. Average weight (g) of mice bearing WM1366 xenografts treated in each cohort (n=5 in control, n=5 in MEKi, n=5 in CDK4/6i, n=6 in COMBOi, error bars represent SD). The weight was comparable between each treatment groups.

Supplemental Figure 10. Modulation of E2F activity in combination treated mice bearing WM1366 xenografts that did not show complete response.

Supplemental Figure 11. E2F reactivation in WM1366 xenografts precedes resistance to MEK inhibitor or CDK4/6 inhibitor as measured by tdTomato activity.

Supplemental Figure 12. Residual tdTomato signal (p/sec/cm^2/sr) in 1205Lu tumors of mice showing complete response by lack of palpable tumor. These five mice were subsequently taken off combination chow treatments to monitor durable response.
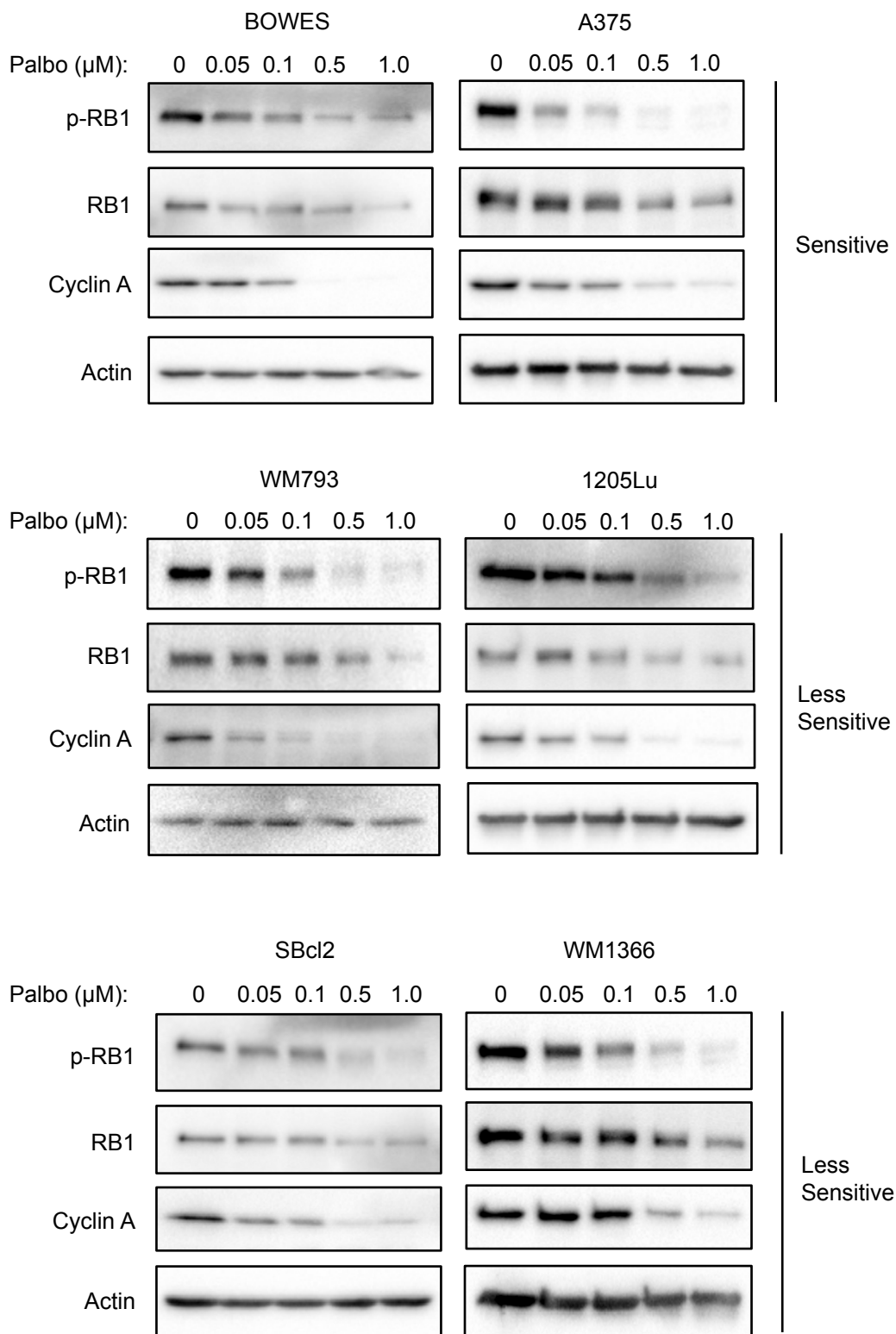
Supplemental Figure 13. Two heat maps of the most significantly up (A) and down (B) regulated pathways for CDK-R vs MEK-R, Combo-R vs MEK-R and Combo-R vs CDK-R (pFDR < 0.001).

Supplemental Figure 14. Validation of proteins from the RPPA analysis heatmap in Figure 6.
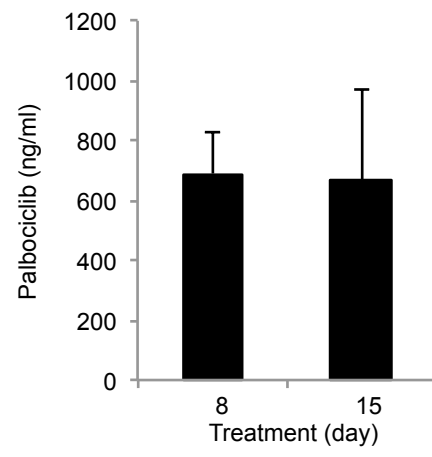
Supplemental Table 1

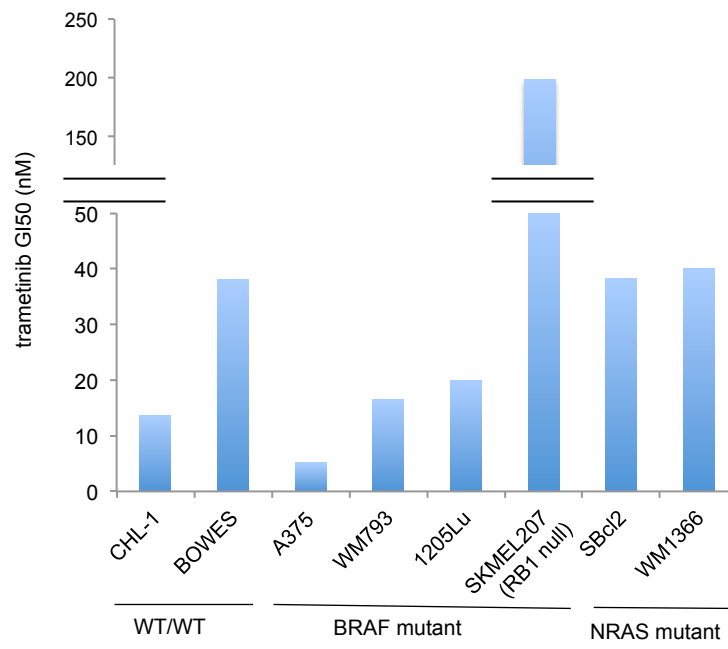| Cell line	Palbociclib (GI50 µM)	CDKN2A (CNV and mutations)	CDK4 mutation	BRAF mutation	NRAS mutation	References
CHL-1	1.15	Mutated (W110Stop, LOF)	WT	WT	WT	Young RJ et al., 2014
BOWES	0.65	SNP	WT	WT	WT	
A375	1.26	Mutated (E61Stop, LOF)	WT	V600E	WT	Young RJ et al., 2014
WM793	3.7	WT	mutated (K22Q)	V600E	WT	Satyamoorthy et al., 1997
1205Lu	10	WT	mutated (K22Q)	V600E	WT	Satyamoorthy et al., 1997
SKMEL207	18.44	WT	mutated (R24C)	V600E	WT	Xing et al., 2012
SBcl2	10	ND	WT	WT	Q61K	Satyamoorthy et al., 1997
WM1366	3.88	ND	WT	WT	Q61L	Satyamoorthy et al., 1997

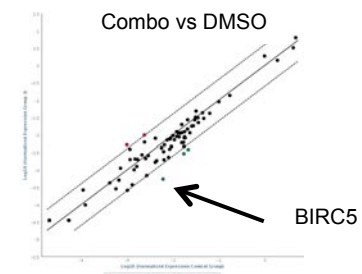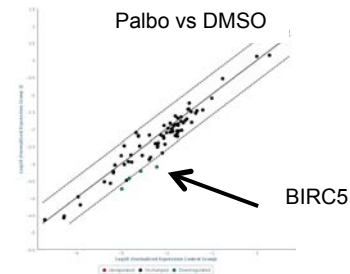Supplemental Figure 1

Supplemental Figure 2

Supplemental Figure 3

Supplemental Figure 4

	CHL-1				BOWES			
Trametinib (5nM)	−	+	−	+	−	+	−	+
Palbo (0.5µM)	−	−	+	+	−	−	+	+

Cleaved PARP

Actin

	WM793				1205Lu			
Trametinib (5nM)	−	+	−	+	−	+	−	+
Palbo (0.5µM)	−	−	+	+	−	−	+	+

Cleaved PARP

Actin

	A375				SBcl2			
Trametinib (5nM)	−	+	−	+	−	+	−	+
Palbo (0.5µM)	−	−	+	+	−	−	+	+

Cleaved PARP

Actin

Supplemental Figure 5

A375

Trametinib vs DMSO

Palbo vs DMSO

BIRC5

Combo vs DMSO

BIRC5

SBcl2

Trametinib vs DMSO

Palbo vs DMSO

BIRC5

Combo vs DMSO
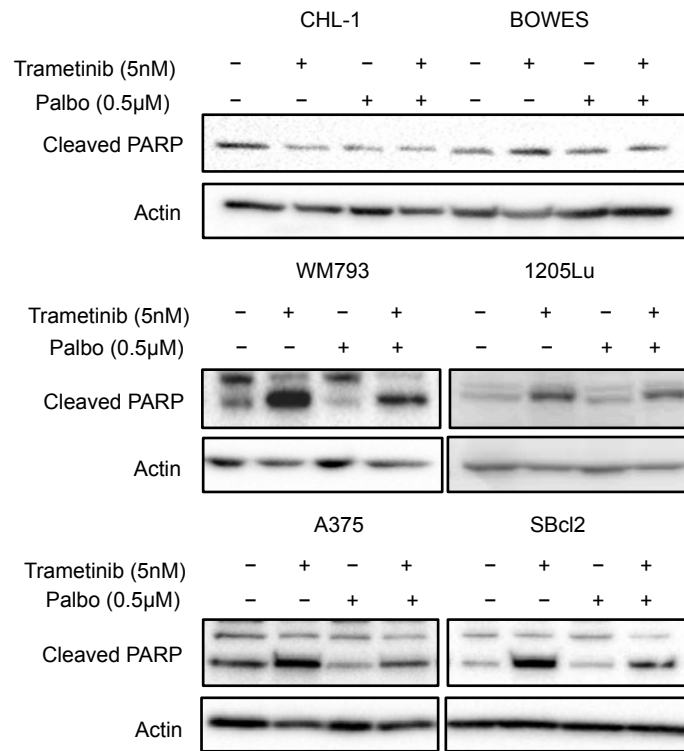
BIRC5

Supplemental Figure 6

1205Lu
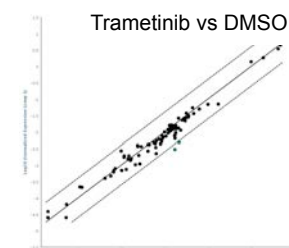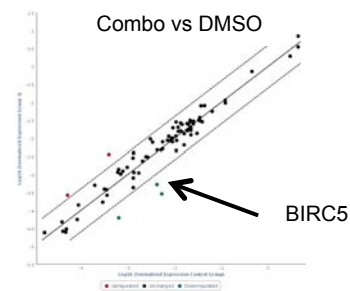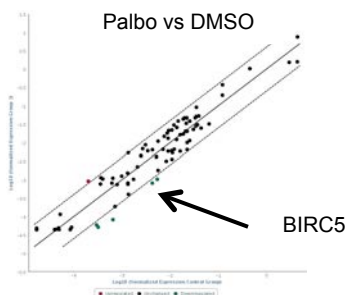
Supplemental Figure 8

Supplemental Figure 9

Supplemental Figure 10

Supplemental Figure 11

Supplemental Figure 12

Supplemental Figure 13

A

B

- log10(pFRD)

AKT phosphorylates targets in the cytosol
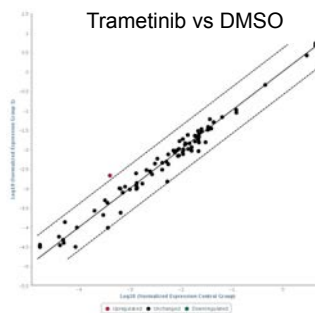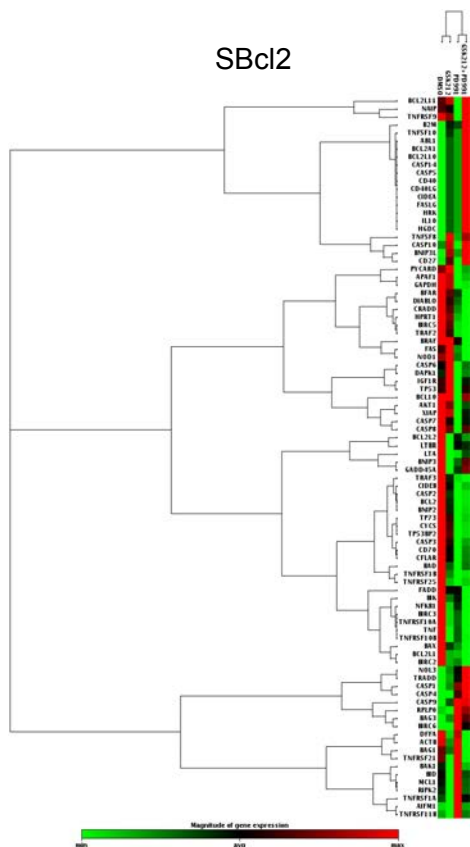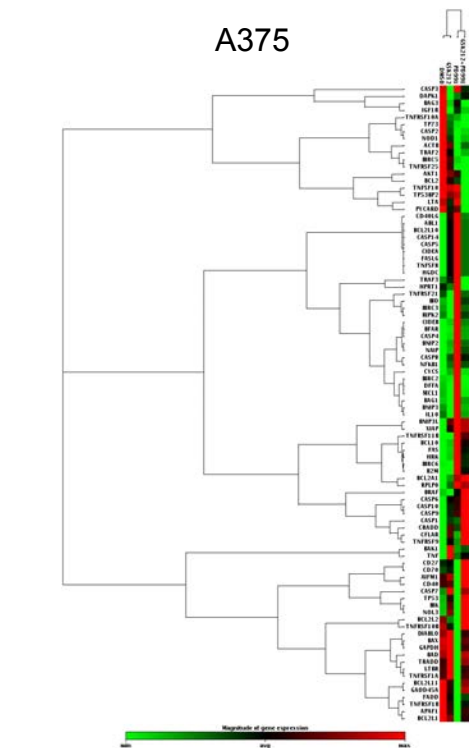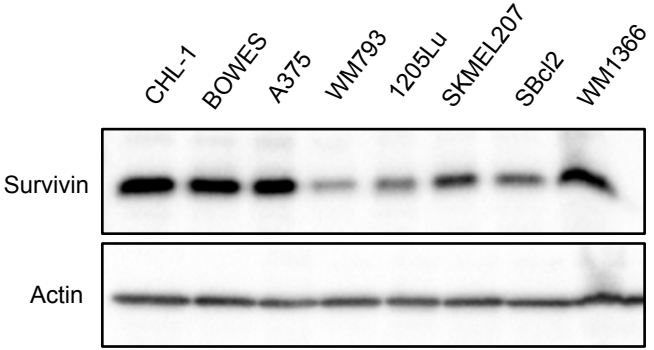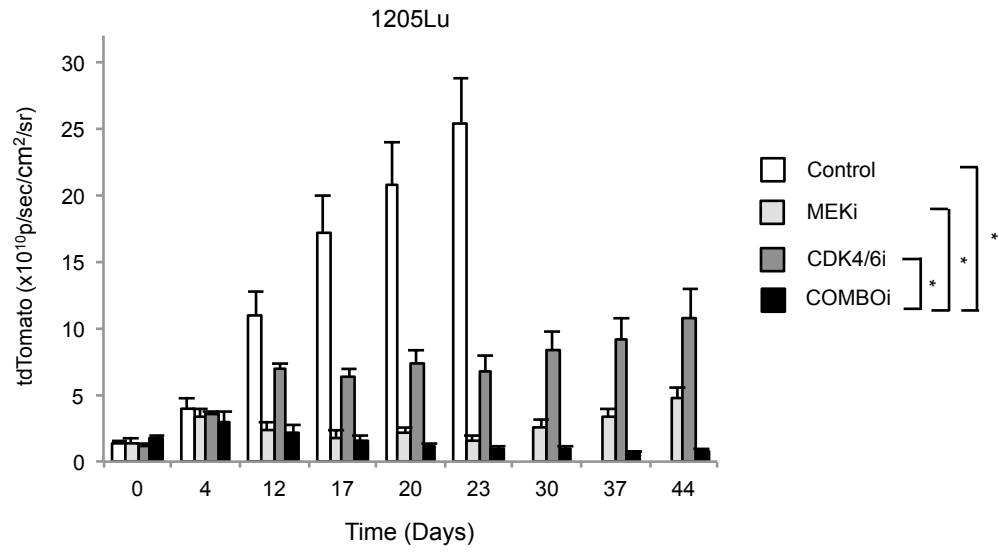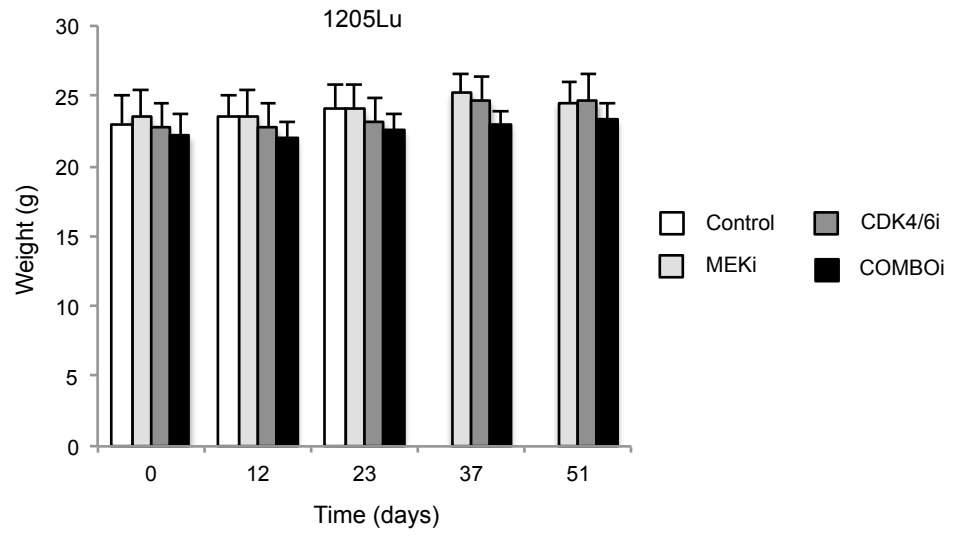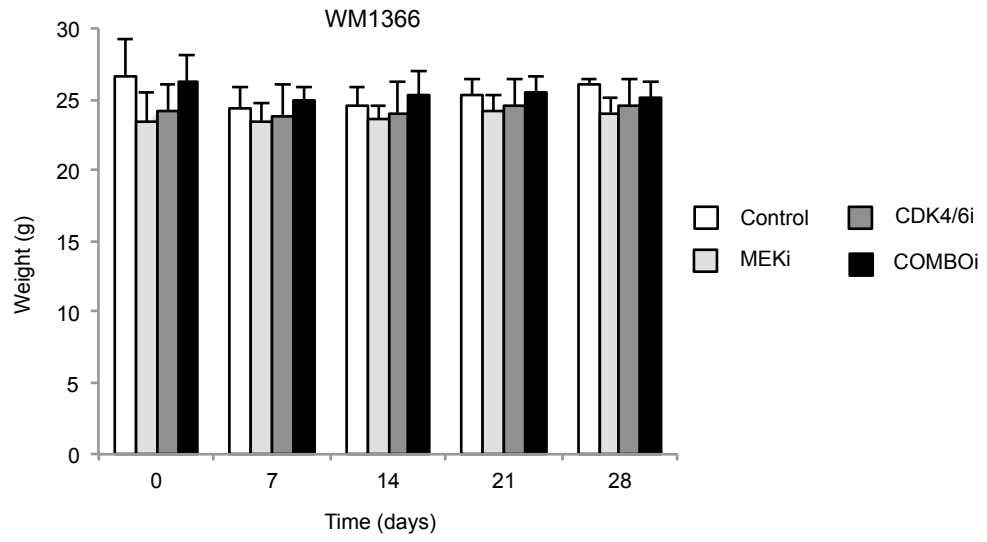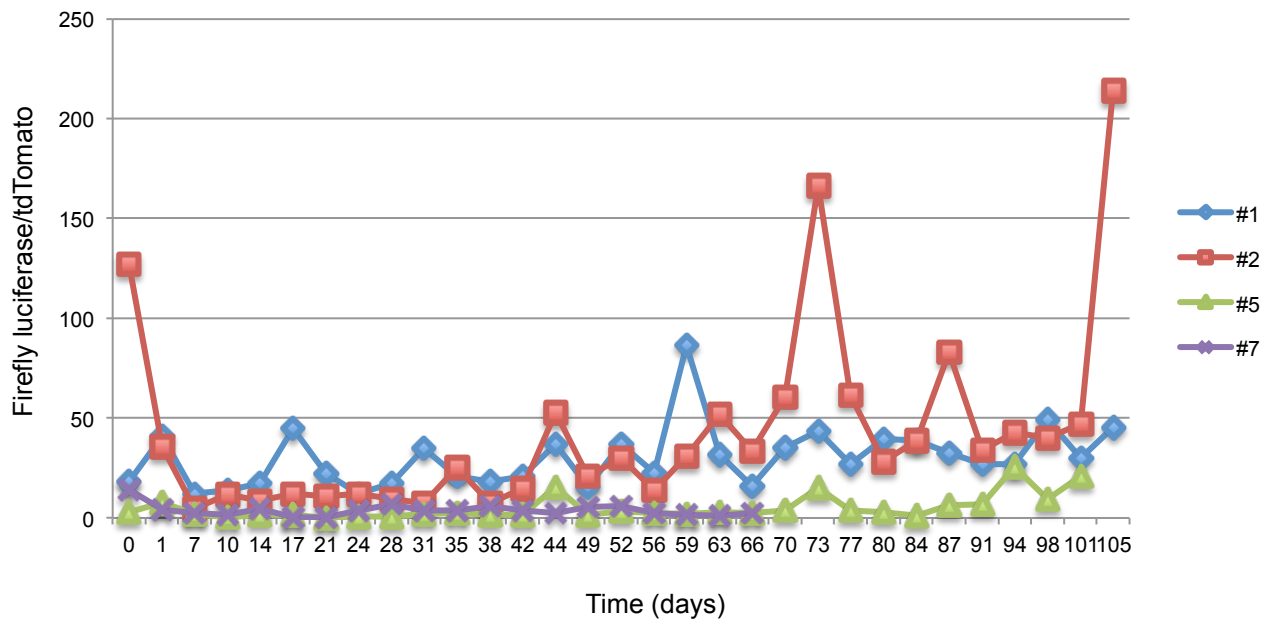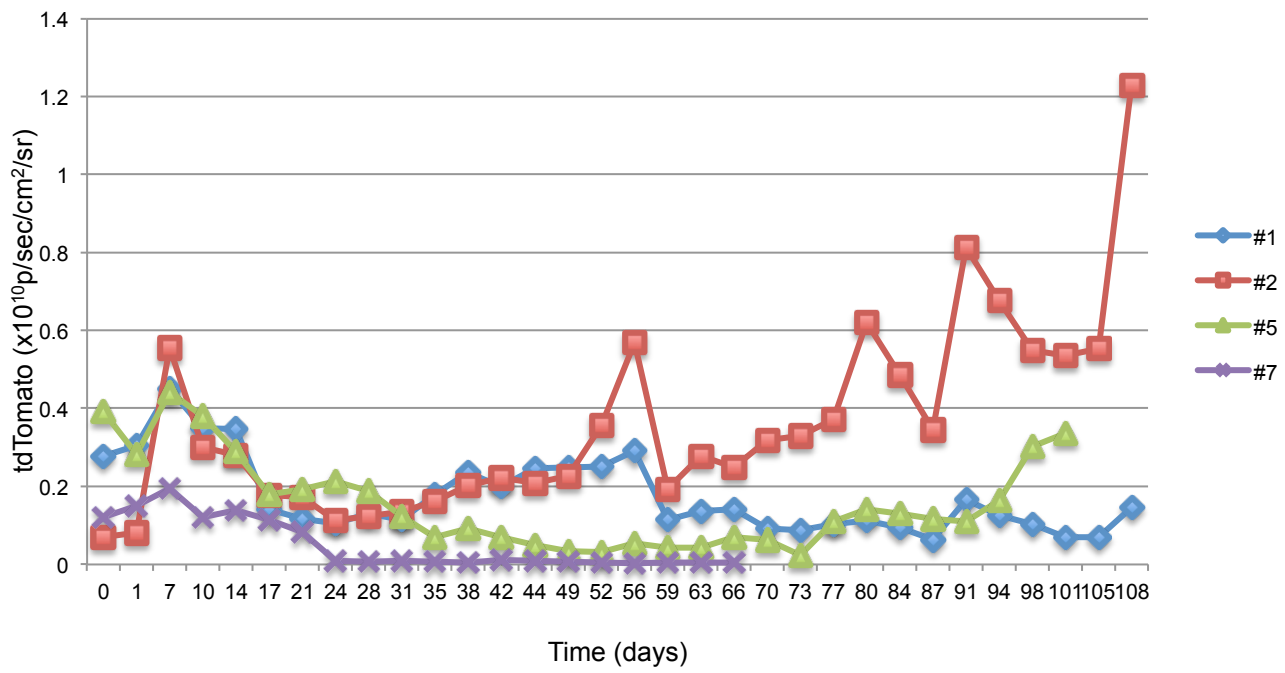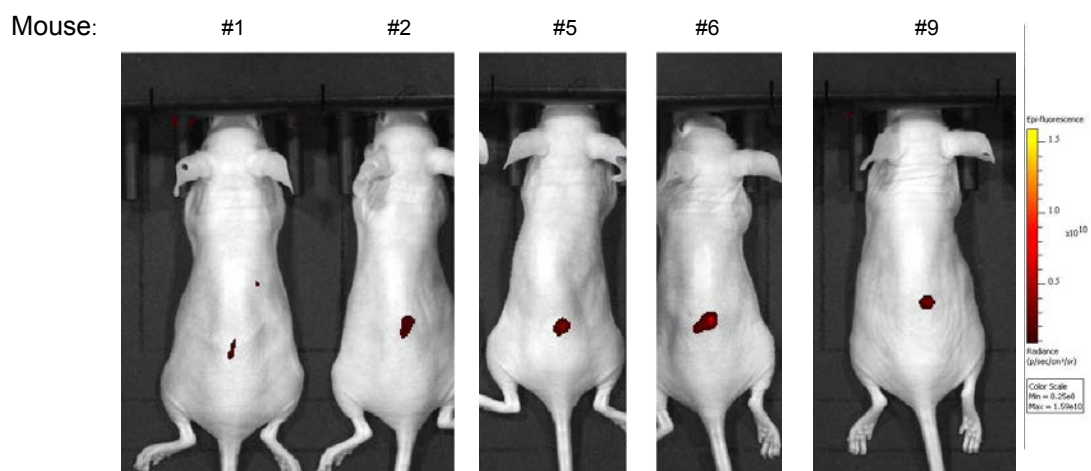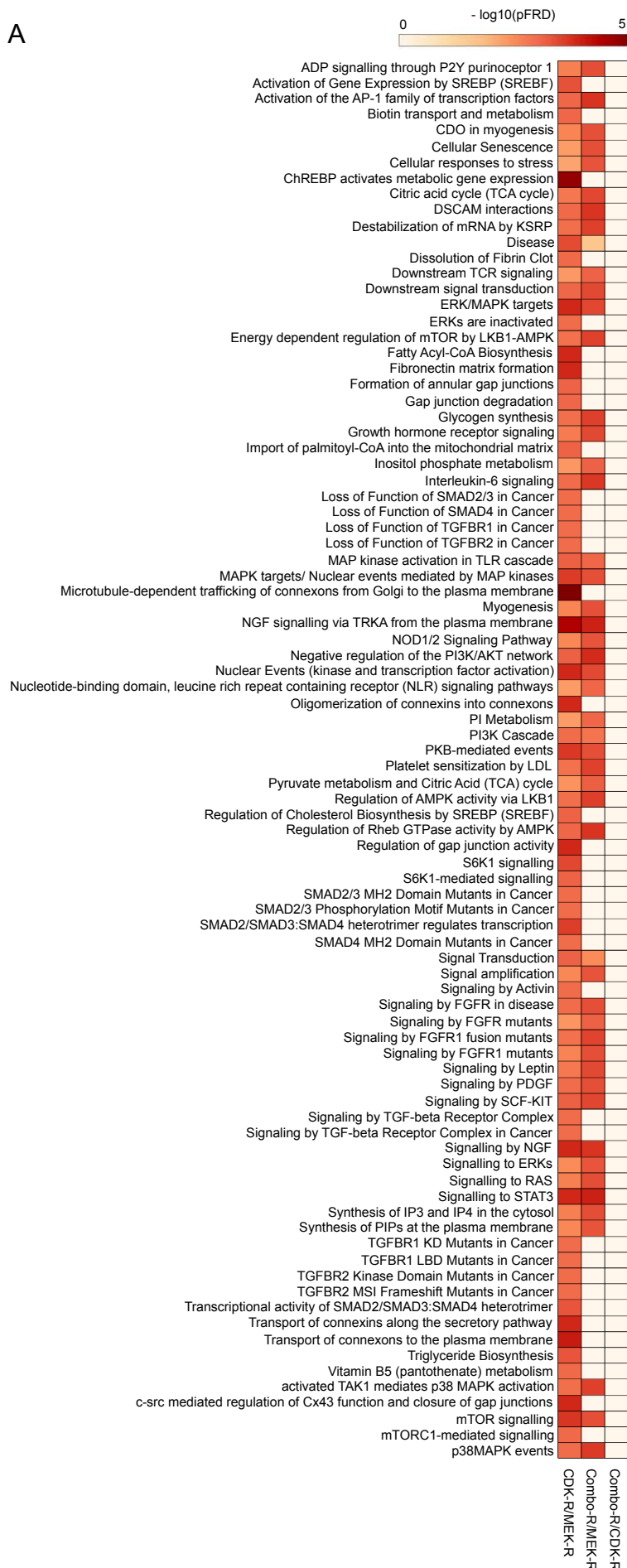AKT phosphorylates targets in the nucleus
AKT-mediated inactivation of FOXO1A
Activation of BAD and translocation to mitochondria
CD28 co-stimulation
CD28 dependent PI3K/Akt signaling
CTLA4 inhibitory signaling
Constitutive PI3K/AKT Signaling in Cancer
Constitutive Signaling by NOTCH1 t(7;9)(NOTCH1:M1580_K2555) Translocation Mutant
Costimulation by the CD28 family
Cyclin A/B1 associated events during G2/M transition
DAP12 interactions
DAP12 signaling
Destabilization of mRNA by Butyrate Response Factor 1 (BRF1)
Destabilization of mRNA by KSRP
Downregulation of ERBB2:ERBB3 signaling
Downregulation of SMAD2/3:SMAD4 transcriptional activity
Downstream Signaling Events Of B Cell Receptor (BCR)
Downstream signal transduction
Downstream signaling of activated FGFR
ERK/MAPK targets
ERKs are inactivated
Fc epsilon receptor (FCERI) signaling
GAB1 signalosome
GRB7 events in ERBB2 signaling
Inhibition of replication initiation of damaged DNA by RB1/E2F1
MAP kinase activation in TLR cascade
MAPK targets/ Nuclear events mediated by MAP kinases
Metabolism of nitric oxide
MyD88 dependent cascade initiated on endosome
MyD88-independent cascade
NGF signalling via TRKA from the plasma membrane
Negative regulation of the PI3K/AKT network
Nuclear Events (kinase and transcription factor activation)
PI-3K cascade
PI3K events in ERBB2 signaling
PI3K events in ERBB4 signaling
PI3K/AKT Signaling in Cancer
PI3K/AKT activation
PIP3 activates AKT signaling
Phosphorylation of proteins involved in G1/S transition by active Cyclin E:Cdk2 complexes
Polo-like kinase mediated events
Regulation of gene expression in beta cells
Release of eIF4E
Role of LAT2/NTAL/LAB on calcium mobilization
SHC1 events in ERBB2 signaling
Signal Transduction
Signaling by EGFR
Signaling by EGFR in Cancer
Signaling by ERBB2
Signaling by ERBB4
Signaling by FGFR
Signaling by FGFR in disease
Signaling by NODAL
Signaling by NOTCH3
Signaling by NOTCH4
Signaling by PDGF
Signaling by SCF-KIT
Signaling by the B Cell Receptor (BCR)
Signalling by NGF
TRAF6 mediated induction of NFkB and MAP kinases upon TLR7/8 or 9 activation
Tetrahydrobiopterin (BH4) synthesis, recycling, salvage and regulation
Toll Like Receptor 3 (TLR3) Cascade
Toll Like Receptor 7/8 (TLR7/8) Cascade
Toll Like Receptor 9 (TLR9) Cascade
eNOS activation
eNOS activation and regulation
mTORC1-mediated signalling

CDK-R/MEK-R
Combo-R/MEK-R
Combo-R/CDK-R

Supplemental Figure 14